Volume 45
Number 31
21 August 2021
Pages 13651–14240

NJC

New Journal of Chemistry

A journal for new directions in chemistry

rsc.li/njc

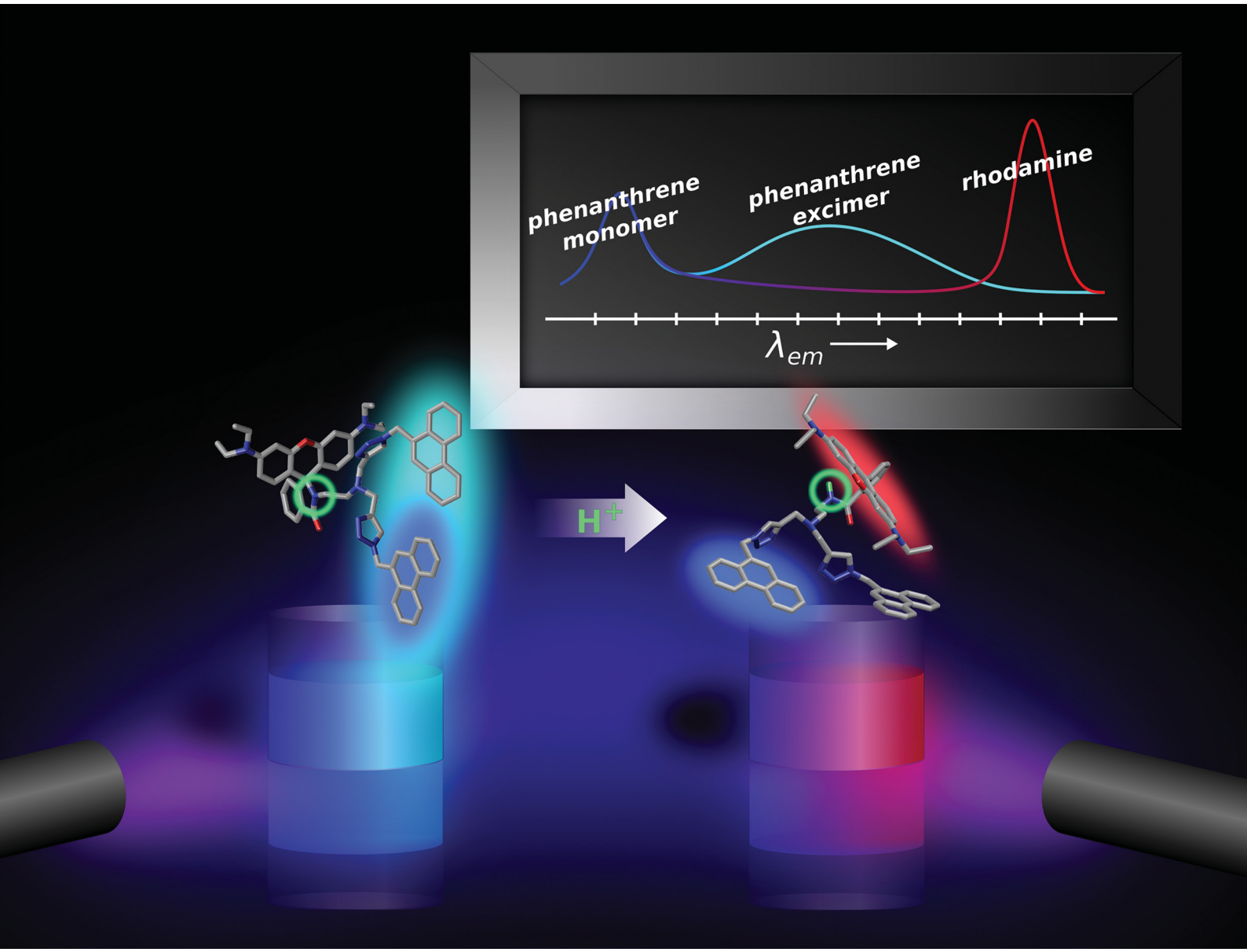

ISSN 1144-0546

ROYAL SOCIETY OF CHEMISTRY

PAPER

Priyanka Srivastava, Ute Resch-Genger *et al.*
Synthesis and spectroscopic characterization of a fluorescent phenanthrene-rhodamine dyad for ratiometric measurements of acid pH values

cnrs

NJC

ROYAL SOCIETY OF CHEMISTRY

PAPER

View Article Online
View Journal | View Issue

Cite this: *New J. Chem.*, 2021, 45, 13755

Synthesis and spectroscopic characterization of a fluorescent phenanthrene-rhodamine dyad for ratiometric measurements of acid pH values†

Priyanka Srivastava, *[a] Paul Christian Fürstenwerth,[a] Jan Felix Witte [b] and Ute Resch-Genger *[a]

We present the rational design, synthesis and spectroscopic characterization of a novel dual excitation, three color emitting, pH-responsive fluorescent probe consisting of two phenanthrene and one rhodamine B units linked by click chemistry. The rhodamine moiety, excitable at λ_{Ex} = 315 nm and at λ_{Ex} = 560 nm in its ring-opened form, provides the pH-responsive fluorophore, while the pH-insensitive phenanthrene, excited at λ_{Ex} = 315 nm, serves as inert internal reference, The presence of two phenanthrene moieties enables a blue monomer and a blueish green excimer emission at 351 nm and 500 nm, respectively. Opening of the rhodamine B spirolactam ring at an acidic pH below 5.0 (pK_a = 2.59 ± 0.04) switches on its emission at 580 nm. Simultaneously, the phenanthrene excimer emission decreases caused by a change in orientation of the phenanthrene units, while the monomer emission is barely affected. This sensor design enables ratiometric measurements in the low acidic pH range utilizing the intensity ratios of the rhodamine B and phenanthrene excimer emission at 580 nm and 500 nm. Alternatively, also the intensity ratios of the rhodamine B and the phenanthrene monomer emission could be exploited or the sum of the phenanthrene monomer and excimer fluorescence. To the best of our knowledge, this is the first report of ratiometric sensing utilizing such a versatile type of tricolor emissive dyad probe bearing phenanthrene moieties and showing phenanthrene monomer and excimer emission.

Received 31st March 2021,
Accepted 8th June 2021

DOI: 10.1039/d1nj01573g

rsc.li/njc

Introduction

pH is one of the most relevant parameters in the life and material sciences indicating *e.g.* proper functioning of cells, diseases like inflammation and cancer, and corrosion processes.[1] Also, pH regulates several metabolic pathways that include endocytic processes, signaling, apoptosis and cell defense mechanisms.[2–5] An acidic environment is for example essential for the functioning and activation of various enzymes and process involved in protein degradation, and organelles like lysosomes (pH 4.5–5.5) and endosomes (pH 4.5–6.8) have an acidic pH for proper functioning.[6–12] Abnormalities in intracellular pH can affect the various cell functions, like muscle contraction and relaxation,[6] apoptosis,[13,14] ion transport, and cellular homeostasis and signal or accompany several diseases including cancer and neurodegenerative disorders.[6,13,14]

pH can be measured electrochemically or optically,[15,16] in the latter case utilizing an optical probe, *i.e.*, a sensor molecule or a chemodosimeter, that signals changes in pH by changes in its absorption[1] and/or fluorescence properties.[17–20] Very sensitive pH measurements with a high spatiotemporal resolution can be best done with pH-responsive molecular or nanoscale optical probes[20–26] which can be also exploited for intracellular pH studies.[1] Suitable pH-responsive probes can be rationally designed utilizing different signaling mechanisms such as (intramolecular) charge transfer, photo-induced electron transfer (PET), or energy transfer (ET)[27–30] processes, that provide the basis for reversible pH-induced changes in the spectral and/or intensity of the probe's absorption and/or fluorescence.[2] Alternatively, a chemical reaction to form an optically detectable species can be exploited.[31] In addition, suitable probes should be chemically stable, show high molar absorption coefficients, and high fluorescence quantum yields as a prerequisite for a high sensitivity. Moreover, they should reveal no or only very little interferences with other analytes such as metal ions typically present in biological systems. As fluctuations of the excitation light source and changes in probe concentration induced by, *e.g.* photobleaching can directly affect measured

[a] *Division Biophotonics, Federal Institute for Materials Research and Testing (BAM), Richard-Willstatter-Strasse, 11, 12489 Berlin, Germany. E-mail: priyanka.srivastava@bam.de, ute.resch@bam.de*
[b] *Institute of Chemistry and Biochemistry, Freie University Berlin, Kaiserswerther Str. 16-18, 14195 Berlin, Germany*

† Electronic supplementary information (ESI) available: Synthesis, characterization of and photophysical data. See DOI: 10.1039/d1nj01573g

fluorescence intensities, pH-responsive probes are favored that enable ratiometric pH measurements. This can be realized with molecules showing a dual emission which is, however, rare,[32–35] or which exhibit strong pH-induced spectral changes in absorption as revealed *e.g.*, by the near-infrared emissive pH-probe Cypher 5.[36,37] Alternatively, two spectrally distinguishable fluorophores can be combined to a ratiometric sensor. This can be achieved with bichromophoric or dyad-type molecular probes,[32–35] that are, however, challenging to synthesize, or with the aid of nanoparticles doped and labeled with two different fluorophores.[38]

A dye class that is particularly well suited for the design of fluorescent probes are the rhodamines. Also, rhodamines can reveal an acid-induced ring opening mechanism occurring at pH values of ~5–4 that provides the basis for OFF–ON fluorescence switching.[26,31] Such an OFF–ON or ON–OFF signaling mechanism, however, does not enable ratiometric, *i.e.*, self-referenced fluorescence measurements. In order to utilize this acidic ring opening mechanism of rhodamine dyes for the design of a ratiometric sensor for pH measurements,[25–31] we designed a novel dyad probe by combining a pH-responsive rhodamine B derivative with two pH-inert phenanthrene fluorophores in one molecule. Phenanthrene was used here since it can form emissive excimers and can provide a blue monomer and a green excimer emission at the same time which can be both used as a reference of the pH-responsive rhodamine emission. Thereby, the dyad probe is always fluorometrically detectable even when the rhodamine fluorophore is in its non-emissive spirolactam form. In the following, we present the synthesis of this first example of a bichromophoric, three color-emissive ratiometric pH probe and its spectroscopic properties as well as selectivity studies.

Results and discussion

Design and synthesis of the pH-sensitive tri-color emissive dyad 8

The synthesis of the bichromophoric pH sensor **8**, obtained from two phenanthrene and one rhodamine B units *via* Click chemistry, is summarized in Fig. 1.[39] A detailed description of the preparation procedures of the different intermediates and the challenging purifications is given in the (ESI†). The synthesis of the azide derivative of phenanthrene starting from phenanthrene carboxaldehyde **1** involves three steps. First, the carboxaldehyde phenanthrene derivative **1**, was reduced to its hydroxy derivative **2**, then a chlorine substituent was introduced by reaction with $SOCl_2$ yielding **3**, and in next step, substituted by an azide group by reaction with NaN_3 in dimethylformamide providing **4**. The propargyl derivative of rhodamine B, compound **7**, was prepared in two steps. In the first step, rhodamine B, *i.e.*, **5**, was reacted with ethylene diamine in ethanol to form the spirolactam ring derivative **6** of rhodamine B with one free amino group. In the second step, the free amine group of **6** reacted with two moles of propargyl bromide to compound **7**. Compound **7** was purified by column chromatography using neutral aluminium oxide to give a faintly yellow resin. Finally, two phenanthrene azide **4** molecules and one molecule of propargyl derivative **7** were coupled by a Click reaction in the presence of $CuSO_4$ and sodium ascorbate in an ethanol water mixture [36] to form pH sensor **8** with a yield of 50%. Comp **8** was purified by column chromatography on neutral Al_2O_3 using a mixture of hexane, ethyl acetate, and methanol as an eluent. Purified **8** was characterized by ^{1}HNMR, ^{13}C NMR, and ESI-MS analysis (Fig. S1–S10, ESI†).

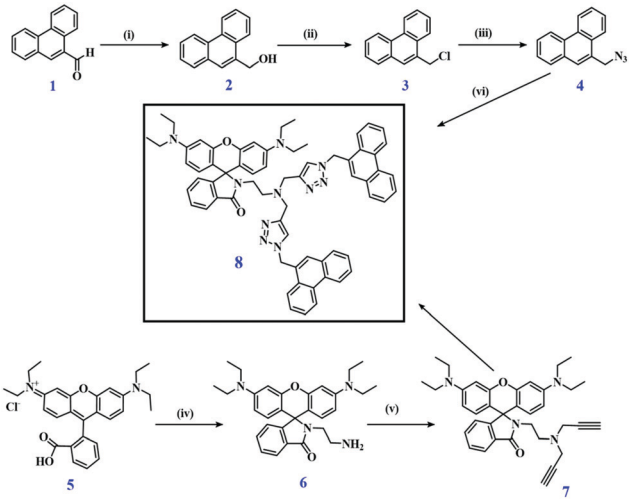

Fig. 1 Synthetic scheme of pH-responsive dyad **8** (i) $NaBH_4$/methanol/RT (ii) $SOCl_2$/DCM/RT (iii) NaN_3/DMF/100 °C (iv) ethylene diamine/ethanol/reflux (v) propargyl bromide/K_2CO_3/THF/reflux (vi) $CuSO_4{\cdot}5H_2O$, sodium ascorbate/ethanol–water/70 °C.

Dyad **8** is designed to exploit the pH-induced ring opening mechanism of the rhodamine spirolactam unit,[26,40–45] that turns this initially colorless and non-emissive moiety into a strongly absorbing pink fluorophore, and combine this ON/OFF pH-sensing with the pH-inert fluorescence of phenanthrene. Phenanthrene was used as this dye can form emissive excimers spectrally distinguishable from the monomer emission, Excimer formation requires the interaction of two neighboring phenanthrene molecules that is favored by the chemical structure of **8**. Thereby, fluorescence intensity-based sensing is combined with the blue monomer and green excimer emission of phenanthrene for single wavelength excitation. Our ratiometric approach for pH sensing utilizes the ratio of the two emission bands of the dyad observed upon excitation at 315 nm, measured in the wavelength range of 420–540 nm and 540–620 nm.

Photophysical behavior of dyad 8

The absorption spectra of dyad **8** in dichloromethane (DCM), tetrahydrofuran (THF), and ethanol (EtOH) reveal absorption bands at 298 nm and 315 nm originating from the phenanthrene and rhodamine moieties, respectively. The corresponding emission spectra recorded at an excitation wavelength (λ_{Ex}) of 315 nm exhibit phenanthrene monomer and excimer emission bands (Fig. 2a and b). At neutral or basic pH to the colorless and non-emissive spirolactam form of rhodamine B derivative **6**, absorbing below 350 nm, is fluorometrically silent. The phenanthrene excimer fluorescence is most pronounced in DCM where the monomer emission is absent. In THF, the excimer emission still exceeds the

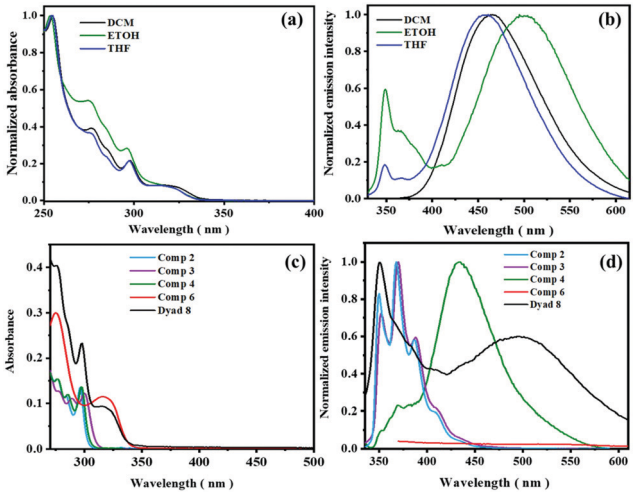

Fig. 2 (a) Normalized absorption and (b) normalized emission spectra of dyad **8** (5 μM) in different solvents (λ_{Ex} = 315 nm; DCM, THF, EtOH). (c) Absorption (8.0 μM) and (d) normalized emission spectra of compounds **2**, **3**, **4**, **6**, and dyad **8** in THF–H_2O mixtures (1 : 1) in a Britton–Robinson (B–R) buffer (25 mM).

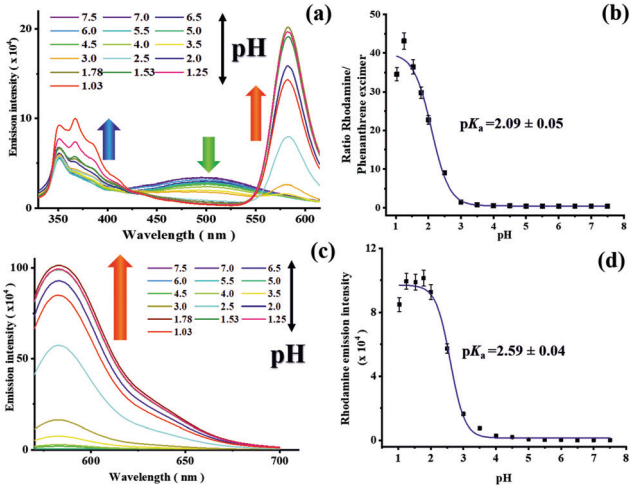

Fig. 3 Emission spectra of dyad **8** (5 μM) at different pH values varied from 7.5 to 1.0 (a) excitation at λ_{Ex} = 315 nm and (c) excitation at λ_{Ex} = 560 nm, respectively. Calculation of the pK_a was done by a sigmoidal fit of (b) a ratiometric approach (readout of I_{582}/I_{500} nm at λ_{Ex} = 315 nm) and (d) for the emission intensity at 580 nm recorded at λ_{Ex} = 560 nm, thereby solely exciting the rhodamine unit. All measurements were done in THF–H_2O solvent mixtures (1 : 1) in a B–R buffer (25 mM).

weak monomer emission, and in ethanol, excimer and monomer fluorescence are equally intense (Fig. 2a, b and Fig. S11, ESI†). For some phenanthrene derivatives, a modest solvent dependence of the optical properties was reported in low or medium polar solvents similar to some reports on the spectroscopic features of pyrene and naphthalene.[46,47] Our dyad molecule reveals shifts in emission in DCM and THF similar to reports from other research groups whereas the red shift observed in the highly polar solvent ethanol is unusual.[48] The spectral position of the monomer emission of the dyad is independent of solvent polarity while the spectral position of the excimer fluorescence undergoes modest changes for low and medium polar solvents and a strong red shift in highly polar protic solvents like ethanol as shown in Table 1. The absorption spectrum of compound **8** is barely affected by solvent polarity.

Table 1 Absorption maxima ($\lambda_{max,Abs}$) and emission maxima ($\lambda_{max,Em}$) of pyrene (used as quantum yield standard; quantum yield value taken from ref. 49 and 50) and compounds **2**, **3**, and **4** as well as dyad **8** in different solvents. all phenanthrene derivatives are excited at 300 nm. The absorbances at the excitation wavelengths were typically between 0.1 and 0.2. The fluorescence quantum yields of the phenanthrene unit in dyad 8 are considerably underestimated in all cases upon excited at 315 nm as the absorbance at this wavelength contains also considerable contributions from the non-emissive ring-closed rhodamine unit as shown in Fig. 2c

Sample	Solvent	Refractive index	$\lambda_{max,Abs}$/ nm	$\lambda_{max,Em}$/ nm	Quantum yield Φ
Pyrene[49,50]	Cyclohexane (CH)	1.42662	333	384	0.320
Compound **2**	THF–water (1 : 1)	1.3801	298	367	0.214
Compound **3**	THF–water (1 : 1)	1.3801	301	370	0.034
Compound **4**	THF–water (1 : 1)	1.3801	296	434	0.067
Dyad **8**	THF–water (1 : 1)	1.3801	315	351, 500	0.026
Dyad **8**	THF–water (2 : 1)	1.3801	315	350, 499	0.039
Dyad **8**	THF–water (1 : 2)	1.3801	315	353, 503	0.024
Dyad **8**	DCM	1.4241	315	466	0.141
Dyad **8**	Ethanol	1.36	315	501	0.025
Dyad **8**	THF	1.4072	315	458	0.086

The absorption and emission spectra of all compounds synthesized for the preparation of dyad **8** are provided in Fig. 2c and d and their quantum yields are given in Table 1. Further studies of this dyad were performed in a mixture of 50% THF and H_2O in a Britton Robinson (B–R) buffer for pH control (ESI†). The absorption spectra of dyad **8** reveal absorption bands at 298 nm and 315 nm (ε = 11 430 M^{-1} cm^{-1}; Fig. S13, ESI†) and the emission spectra (λ_{Ex} = 315 nm) exhibit two bands at 351 nm and 500 nm (overall quantum yield of both phenanthrene emission bands Φ = 0.026; 65% and 35% contribution from phenanthrene excimer and monomer emission) as shown in Fig. 3. Please not here that the fluorescence quantum yields of the phenanthrene unit in dyad **8** are considerably underestimated upon excitation at 300 nm as the absorbance at this wavelength contains also considerable contributions from the non-emissive ring-closed rhodamine unit as shown in Fig. 2c.

pH studies of dyad 8

The absorption and emission properties of dyad, **8** (5 μM) were studied in the pH range of 7.5 to 1.0 in THF–H_2O mixtures (1 : 1) in a Britton Robinson buffer[51] using excitation wavelengths of 315 nm (phenanthrene and rhodamine absorption) and 560 nm (rhodamine absorption), thereby examining also the pH-dependence of the emission behavior of the different fluorophores constituting the dyad sensor. Excitation at 315 nm results in two emission bands at λ_{Em} = 351 nm and λ_{Em} = 500 nm at pH 7.5 originating solely from the phenanthrene moieties as the rhodamine exists in its ring-closed form under these conditions that is non-emissive. A change in pH from 7.5 to 4.5 barely affects the intensity of both the phenanthrene monomer and excimer emission indicating the suitability of phenanthrene as pH-inert reference dye. A further decrease of

Table 2 Fluorescence quantum yields of dyad **8** and compound **6** at pH 7.0 and pH 2.0 with pyrene (pyrene in cyclohexane: Φ = 0.32; ref. 49 and 50) and rhodamine B (rhodamine in ethanol: Φ = 0.7; ref. 53) as quantum yield standards determined at different excitation wavelengths. The absorbances of the samples at the excitation wavelength were between 0.1 and 0.2. The emission range given equals the emission range used for integration of the fluorescence bands

Sample	Solvent	Refractive index	Emission range/nm	$\lambda_{max,Abs}$/nm	$\lambda_{max,Em}$/nm	Quantum yield Φ
Pyrene[49,50]	CH	1.42662	350–600 nm	335		0.32
Dyad **8** pH 7.0	THF–water (1 : 1)	1.3801	330–620 nm	315	351, 500	0.026[a]
	THF–water (1 : 1)	1.3801	330–540 nm		351, 500	0.022
	THF–water (1 : 1)	1.3801	540–620 nm		580	0.004
Dyad **8**, pH 2.0	THF–water (1 : 1)	1.3801	330–620 nm	315	351, 580	0.045
	THF–water (1 : 1)	1.3801	330–540 nm		351	0.017
	THF–water (1 : 1)	1.3801	540–620 nm		580	0.028
Compound **6** pH 2.0	THF–water (1 : 1)	1.3801	540–620 nm	315	580	0.061
Rhodamine B[46]	Ethanol	1.360	565–750 nm	543	590	0.7
Dyad **8** pH 2.0	THF–water (1 : 1)	1.3801	570–750 nm	560	582	0.451
Compound **6** pH 2.0	THF–water (1 : 1)	1.3801	570–750 nm	560	582	0.507

[a] 35% contribution monomer; 65% excimer.

the pH from 4.5 to 2.0, however, leads to a diminution particularly of the phenanthrene excimer emission at 500 nm and the appearance of a new fluorescence band at 582 nm corresponding to the rhodamine B derivative with the open spirolactam ring (Table 2 and Fig. 4, Table S1, ESI†). The intensity of this band further increases with decreasing pH (Fig. 3a and Fig. S14, ESI†) and saturates at pH 1.78. The ratiometric response (I_{582}/I_{500} nm) of the fluorescence intensities of the rhodamine B and phenanthrene excimer of the dyad sensor at different pH yields a pK_a as 2.09 ± 0.05 (Fig. 3b; λ_{Ex} = 315 nm) by applying a dose response equation for the sigmoidal fit of the pH curve.[52]

The influence of pH on the spectroscopic properties of **8** was also assessed for an excitation wavelength of 560 nm, where solely the rhodamine B moiety absorbs. At pH 7.5 the spirolactam rhodamine B derivative absorbs only at wavelengths <350 nm (see Fig. 2, compound **6**) and is not emissive. As the pH decreases further to pH 6.0, a new absorption band at about 560 nm appears and a new emission band at 582 nm. The intensity of both bands is gradually enhanced at more acidic pH values (Fig. 3c). A further decrease of pH leads to a large fluorescence enhancement. The fluorescence quantum yield of the resulting ring opened rhodamine B amounts to Φ = 0.45 (pH 2.0). The pK_a value of the rhodamine system is calculated to pK_a = 2.59± 0.04 utilizing a dose response equation (Fig. 3d; rhodamine excitation at 560 nm).

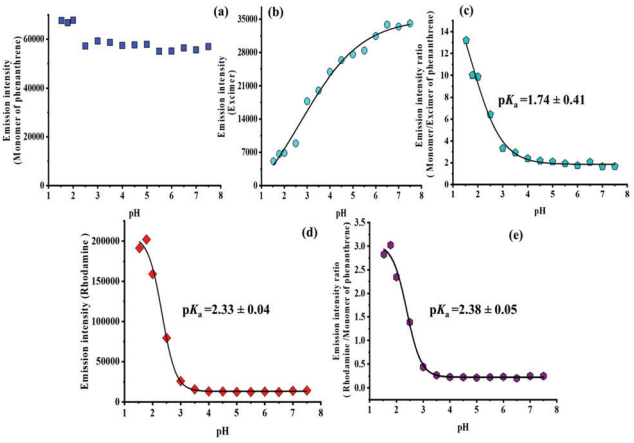

Fig. 4 Emission intensity changes of dyad **8** (λ_{Ex} = 315 nm) as a function of pH shown for (a) the 351 nm emission of the phenanthrene monomer, (b) the 500 nm fluorescence of the phenanthrene excimer, (c) the intensity ratio of the phenanthrene monomer and excimer emission at 351 nm and 500 nm, (d) the 582 nm rhodamine emission, and (e) the intensity ratio of the 582 nm rhodamine and the 351 nm phenanthrene monomer fluorescence. All measurements were done with dyad **8** dissolved in THF–H_2O mixtures (1 : 1) in a B–R buffer (25 mM).

The pH-dependence of the three different emission bands of dyad **8** observed upon 315 nm excitation was subsequently studied in more detail. The pH-dependence of the emission bands at 351 nm, 500 nm, and 582 nm is shown in Fig. 4 for the pH range of 7.5 to 1.5. The monomer emission undergoes only minimum intensity changes up to a pH of 2.0 (Fig. 3 and 4a) and can serve as a constant pH-inert reference to monitor the changes exhibited either by the excimer fluorescence of phenanthrene at 500 nm (see Fig. 3 and 4b) or the rhodamine emission intensity at 582 nm (Fig. 3 and 4d). The intensity ratio of the phenanthrene monomer and excimer fluorescence (Fig. 4c) showed a pK_a = 1.74 ± 0.41 (351/500 nm) while the intensity ratio (Fig. 4e) of the rhodamine emission at 582 nm and the phenanthrene monomer fluorescence at 351 nm revealed a pK_a = 2.38 ± 0.05 (582/351 nm). A plot of the intensity of the 582 nm rhodamine emission excited at 315 nm as a function of pH gives a pK_a = 2.33 ± 0.04 (Fig. 4d).

The response time of dyad 8 to pH was determined by addition of dyad **8** to a THF–water solution of pH 2.0 (Fig. 5). The emission spectra of the dye measured immediately after addition (0 min) showed a complete disappearance of the excimer emission. Subsequently, the rhodamine emission band at 582 nm started to appear and increased steadily in intensity with time. After 16 min, only marginal changes were observed, and the emission spectra reached constant values about at 20 min. Hence, although the overall response time of dyad **8** for a complete ring opening is 20 min. at pH 2.0 as reflected by constant emission spectra resulting at this time, the appearance and growing in of the rhodamine emission started

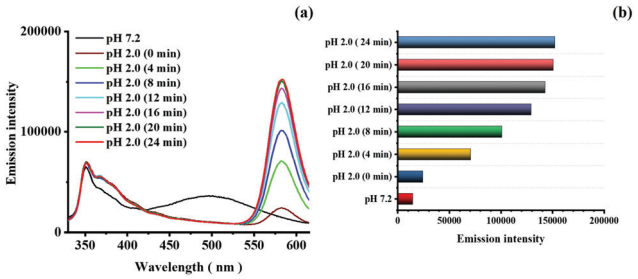

Fig. 5 (a) Emission spectra and (b) bar graph of the response time of the fluorescence of dyad **8** observed upon addition of dyad **8** to a THF–H_2O mixture (1 : 1) in B–R buffer (25 mM) of pH 2.0; excitation λ_{Ex} was at 315 nm and the fluorescence intensity was recorded at an emission wavelength λ_{em} of 582 nm. The emission spectra of dyad **8** were recorded every 4 min. The data obtained at pH 7.2, where no ring opening should occur, are included as control.

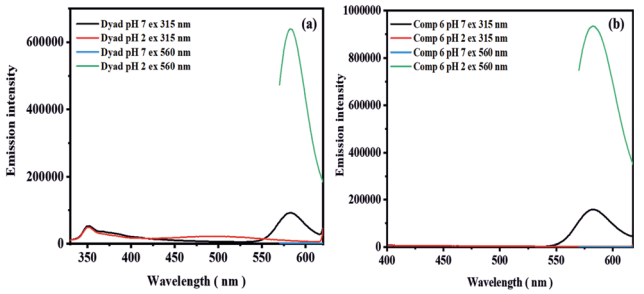

Fig. 6 Emission spectra recorded at excitation wavelength of 315 nm and 560 nm at pH 7.0 and 2.0 (3.3 μM) of (a) dyad **8** and (b) compound **6** in a THF–H_2O mixture (1 : 1) in B–R buffer (25 mM).

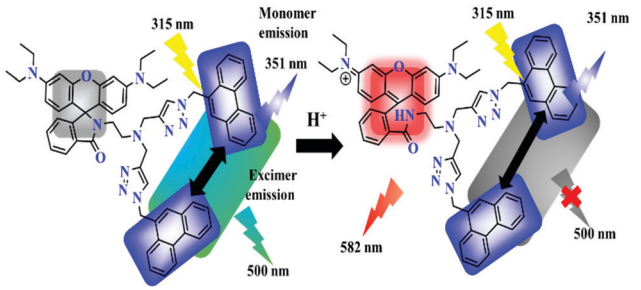

Fig. 7 The spirolactam and open ring derivative of the dyad **8**.

immediately upon dye–proton interaction. This principally provides the basis for shorter measurement times.

Mechanistic studies and considerations

As previously discussed, pH sensing with the rhodamine moiety utilized in dyad **8** is based upon the pH-induced opening of the spirolactam ring of the rhodamine. This ring opening reaction at pH < 5 involves the protonation of the amino group of the xanthene core, which is signaled by the appearance of an absorption band at 560 nm responsible for the pink color of the dyad solution and an increasingly enhanced emission located at 582 nm (Fig. 7). The opening of the spiro-lactam ring simultaneously changes the distance and possibly also the orientation of the two phenanthrene units, which is reflected by a decrease of the phenanthrene excimer emission by about 66%. Although phenanthrene itself is not sensitive to pH as demonstrated by us (Fig. S14, ESI†), this also renders the phenanthrene excimer emission pH-responsive at acidic pH values $\leq$4.5 (Fig. 4b). The decrease in excimer emission automatically leads to an increase in the monomer emission of phenanthrene as shown in Fig. 3 (panel a) by about 23% (Fig. S15, ESI†). These changes barely affect the ratiometric readout of the sensor dyad. Moreover, by utilizing the sum of the monomer and excimer emission of phenanthrene as a reference for the pH-dependent rhodamine emission, *e.g.* by using integral fluorescence intensities (integration of the rhodamine emission from 540 nm to 620 nm; integration of the phenanthrene emission from 330 nm to 540 nm) instead of intensity ratios measured at single wavelengths of 580 nm and 500 nm, these effects can be considered.

Subsequently, we tried to quantify the contribution of the phenanthrene and rhodamine absorption to the dyad's absorption at 315 nm chosen as excitation wavelengths for ratiometric pH measurements. For this purpose, we compared the absorption and fluorescence excitation spectra of dyad **8** and compound **6** (Fig. S16, ESI†). This comparison reveals a ratio of the absorption values at 315 nm and 560 nm at pH 2.0 of 2.9 for dyad **8** while for compound **6** which has only a rhodamine unit, this ratio amounts to only 1.28 (Fig. S17, ESI†). The emission intensity at 582 nm resulting upon excitation at 560 nm exceeds that observed upon excitation at 315 nm by a factor of 6.95 in the case of dyad **8** as shown in Fig. 6 while for compound **6** a factor of 5.86 was obtained under similar experimental conditions. This difference between dyad **8** and compound **6** is ascribed to the presence of the two phenanthrene moieties in the dyad. When considering the fluorescence quantum yields of the 580 nm rhodamine emission band (wavelength range of 540–620 nm) excited at 315 nm and 560 nm, the difference between the two emission ratios obtained at 580 nm of 1.3 correlates with the contribution of the phenanthrene moieties to the absorption of the dyad at 315 nm. Similarly, we observed a 1.33-fold decrease in fluorescence quantum yield of the 580 nm band of the rhodamine (540–620 nm range) excited at 330 nm for dyad **8** in comparison to compound **6** lacking the phenanthrene units (Table 2).

In addition, we performed time-resolved fluorescence studies with dyad **8** and compound **6** at pH 2.0. The resulting fluorescence decay curves are shown in the ESI,† in Fig. S18 and S19. Fitting these decay curves with biexponential decay kinetics provided fluorescence lifetimes τ of 1.71 ns (84%) and 1.66 ns (76%) for dyad **8** of the main decay components using a biexponential fit of the fluorescence decays obtained at excitation wavelengths of 330 nm and 510 nm (detection at 580 nm) and fluorescence lifetimes τ of 1.63 ns (monoexponential fit) and 1.73 ns (84%; main component) for compound **6** (biexponential) for excitation at 330 nm and 510 nm and detection at 580 nm (Fig. S18 and S19, ESI†). The lifetimes are almost similar in the case of dyad **8** and compound **6** indicating the absence of electronic interaction between the rhodamine and phenanthrene units.

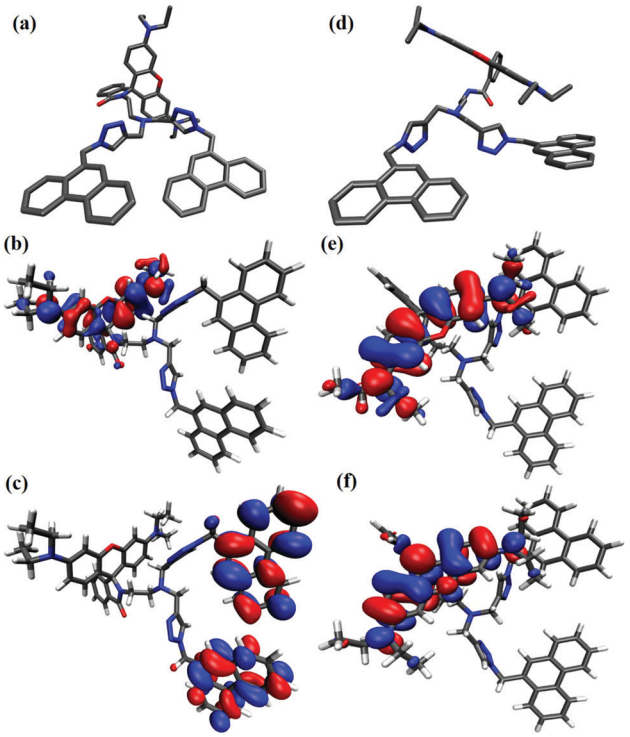

Fig. 8 DFT optimized structures of dyad **8** (a) and its **8** + H^+; protonated form (d); HOMO (b) and LUMO (c) isosurfaces of dyad **8** and protonated form HOMO (e) and LUMO (f) obtained at the ωB97X-D3/def2-TZVP level. Plots were generated using ORBKIT, isovalue = $0.02a_0^{-3}$.[54–57]

Quantum chemical calculations

Dyad **8** and its protonated form have been optimized at the PBEh-3c[54] level of density functional theory (DFT) using the Turbomole programme package (version 7.3)[55] and COSMO[56] to implicitly include solvation effects (Fig. 8). Fig. 8 shows the HOMO and LUMO isosurfaces of dyad **8** and protonated **8** + H^+ obtained at the ωB97X-D3 level. For **8**, the HOMO is localized on the rhodamine structural motif (Fig. 8b), while the LUMO is delocalized over the two phenanthrene moieties (Fig. 8b).[57] The degree of localization in the LUMO is governed by the amount of "exact" exchange included in the density functional approximation that is employed. In the case of PBE0 (20% exact exchange), for example, the LUMO is fairly localized on the phenanthrene units. For protonated dyad [**8** + H^+], both HOMO and LUMO are localized on the rhodamine motif (Fig. 8, panels e and f). A closer inspection reveals that the major difference between the two orbitals is given by the distribution of the nodes at the central pyran unit. Not very surprisingly, while the HOMO contains contributions from a conventional π-orbital located at the pyran moiety, the LUMO encompasses its π*-orbital analogue.

The most useful values are likely acquired with the PBE0 functional which results in a HOMO–LUMO gap of 4.2 eV for **8** and 3.10 eV for **8** + H^+. In general, the HOMO–LUMO gap decreases by roughly 1–1.5 eV when protonating the dyad. The front view of dyad **8** and its protonated form revealed a clear change in the orientation of the phenanthrene units caused by the opening of spirolactam ring of rhodamine B as expected (Fig. 8, panels a and d). The DFT optimized structures also showed an increased in the distance between the two phenanthrene units from 8.92 Å for dyad **8**, and 11.22 Å for the protonated dyad, respectively. As the observed change in distance is not large, we can conclude that the orientational changes of phenanthrene units are responsible for the observed excimer emission decrease at acidic pH values.

Analyte selectivity and photostability

To assess the analyte selectivity of the dyad sensor, we performed selectivity studies in THF–H_2O mixture in B–R buffer with metal ions typically present in biological systems or in other application-relevant environments. Thereby, always 10 equiv (10 fold excess; 50 μM) of different metal ions (K^+, Na^+, Ca^{2+}, Ba^{2+}, Mg^{2+}, Cd^{2+}, Zn^{2+}, Co^{2+}, Ni^{2+}, Cu^{2+}, Hg^{2+}, Fe^{2+}, and Fe^{3+}, 1.5 μL of 10^{-1} M) were separately added to dyad solutions (5 μM) and the resulting emission spectra obtained at λ_{Ex} of 315 nm (phenanthrene excitation) and 560 nm (rhodamine excitation) were measured for each [Dyad + $Metal^+$] solution. These screening studies revealed no significant changes for any of these metal ions as highlighted in Fig. 9 (Fig. S20 ESI†). We also performed selectivity and interaction studies of dyad **8** with different anions and selected amino acids (10 equiv; 1.5 μL of 10^{-1} M). None of these anions or amino acids led to changes in the emission intensity of our dyad as shown in Fig S21 in the ESI.† These results underline the high selectivity of dyad **8** for protons/pH.

The advantage of using phenanthrene as a reference fluorophore follows from the photographs of the sensor solutions. The violet color of phenanthrene is visible at pH 7.5 to 5.5 while the rhodamine signal is absent at pH 7.5 (Fig. 10; left). Thereby, dyad 8 can b always detected fluorometrically which would otherwise not feasible. An acidic pH of 5 or less is signaled by the appearance of the orange-red color of the rhodamine absorption and emission.

Other factors that govern the suitability of a sensor are its response time, reversibility and chemical and photochemical stability. To assess the reversibility and hence reusability of dyad **8**, we ran pH cycles with 8, varying the pH of dyad

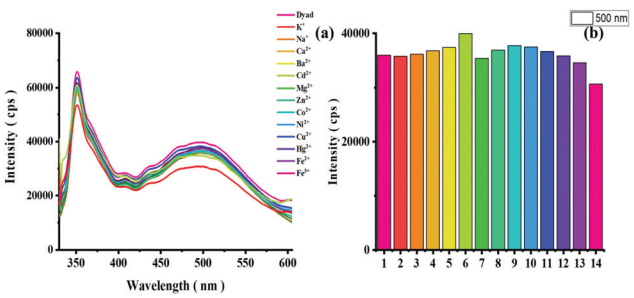

Fig. 9 (a) Emission spectra and (b) bar diagram of the selectivity studies of dyad **8** with the application-relevant metal ions K^+, Na^+, Ca^{2+}, Ba^{2+}, Cd^{2+}, Mg^{2+}, Zn^{2+}, Co^{2+}, Ni^{2+}, Cu^{2+}, Hg^{2+}, Fe^{2+}, and Fe^{3+} always separately adding 10 equiv. (10 fold excess) of the respective metal ion to dyad **8** (5 μM). Excitation was at λ_{Ex} of 315 nm (phenanthrene). in THF–H_2O mixture (1 : 1) in B–R buffer (pH 7.0; 25 mM).

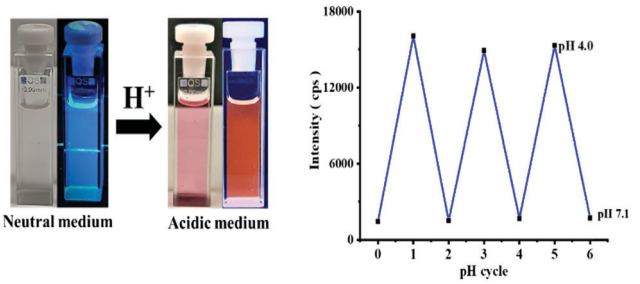

Fig. 10 (a) Color changes of the pH sensor 8 under UV light detected by naked eye at pH 7.0 and pH 2.0; (b) reversibility of the fluorescence response of dyad **8**. All measurements were done with 5 μM of dyad **8** dissolved in a THF–H_2O mixture (1 : 1) in B–R buffer (pH 7.0; 25 mM).

solutions from 7.0 to pH 4.0 back and forth up to three times and measured the fluorescence intensity at 582 nm corresponding to the open ring form of rhodamine B (λ_{Ex} = 560 nm). These measurements did not reveal a loss in fluorescence after these pH cycles (Fig. 10; right). Moreover, the response times are very short, in the order of a few seconds. To determine the photostability of dyad **8**, dyad solutions (5 μM; THF–water solution) of pH 7.2 and pH 2 were illuminated with a 450 W xenon lamp of a fluorometer for up to 420 mins and the emission spectra of **8** were recorded every 30 minutes, using an excitation wavelength of 315 nm. The emission intensities at 350 nm and 500 nm at pH 7.2 and 350 nm and 582 nm at pH 2.0 revealed only marginal changes, underlining the high photostability of our dyad (see ESI,† Fig. S22).

Conclusion

We designed and synthesized a new sensor dyad combining two pH-insensitive phenanthrene fluorophores and one pH-sensitive rhodamine B derivative in one molecule and spectroscopically assessed its pH responsivity in THF–water mixtures in in Britton–Robinson (B–R) buffer in the pH range of 7.5 to 1.0. These studies underline the advantage of our dyad sensor revealing three spectroscopically distinguishable emission bands at 351 nm, 500 nm, and 582 nm upon excitation at a single wavelength of 315 nm, originating from the phenanthrene monomer, phenanthrene excimer and the rhodamine. In comparison to a simple OFF–ON sensor molecule like a fluorescent probe exploiting a photoinduced electron transfer (PET), utilization of the phenanthrene monomer emission or the combined monomer and excimer emission as the pH-inert reference signal enables not only ratiometric measurements for analyte quantification but also the visualization of the dyad at all pH values, also at pH values $\geq$7.5 where the rhodamine is in its ring-closed non-emissive spirolactam form. The use of two phenanthrene units provides more versatility regarding the choice of the reference signal, namely either the blue phenanthrene monomer emission or combined blue and green phenanthrene fluorescence. Screening studies with a series of biologically relevant metal ions underline the excellent selectivity of our pH-responsive dyad.

In the future, we plan to improve the water solubility of our dyad sensor by introducing hydrophilic substituents such as a 2-chloro methane sulfonate substituent. Moreover, to bind the dyad to different types of nanoparticles acting as carriers, this substituent can be used in conjunction with an additional reactive carboxylic group introduced into the rhodamine part of the dyad. For the simple application in aqueous environments dyad **8** without the need for chemical modification, compound **8** can be encapsulated in mesoporous silica nanoparticles[58] or polymer-based nanoparticles like PEBBLE[59] type nanoparticles. This provides also a simple signal enhancement strategy and enables, *e.g.* a straightforward approach to combine dyad **8** with targeting bioligand like biomarker-specific antibodies.[60] Furthermore, the dye can also be integrated into a D4 hydrogel yielding a pH-responsive sensor film as previously done for water-insoluble BODIPY dyes.[52]

Conflicts of interest

There are no conflicts to declare.

Acknowledgements

P. S. acknowledges the Adolf Marten fellowship of the Federal Institute for Material Research and Testing (BAM), Berlin, Germany. F. W. gratefully acknowledges the Deutsche Forschungsgemeinschaft for financial support through research grant PA 1360/16-1. The North-German Supercomputing Alliance (Norddeutscher Verbund für Hoch-und Höchstleistungsrechnen) is acknowledged for providing computational resources. We are also grateful for support by the NMR and mass spectrometry facilities of Freie University Berlin measuring the NMR and MS spectra of the compounds prepared.

Notes and references

1 A. Steinegger, O. S. Wolfbeis and S. M. Borisov, *Chem. Rev.*, 2020, **120**, 12357–12489.
2 H. Izumi, T. Torigoe, H. Ishiguchi, H. Uramoto, Y. Yoshida, M. Tanabe, T. Ise, T. Murakami, T. Yoshida, M. Nomoto and K. Kohno, *Cancer Treat. Rev.*, 2003, **29**, 541–549.
3 M. Chesler, J. O. Brien, A. Zappala, F. Cicirata and L. C. Barrio, *Physiol. Rev.*, 2008, 1183–1221.
4 A. M. Paradiso, R. Y. Tsien and T. E. Machen, *Nature*, 1987, **325**, 447–450.
5 Y. Yue, F. Huo, S. Lee, C. Yin and J. Yoon, *Analyst.*, 2017, **142**, 30–41.
6 J. R. Casey, S. Grinstein and J. Orlowski, *Cell Biol.*, 2010, **11**, 50–61.
7 I. Mellman, R. Fuchs and A. Helenius, *Annu. Rev. Biochem.*, 1986, **55**, 663–700.
8 R. Martinez-Zaguilan, E. A. Seftor, R. E. Seftor, Y. W. Chu, R. J. Gillies and M. J. Hendrix, *Clin. Exp. Metastasis*, 1996, **14**, 176–186.

9 S. Kornfeld and I. Mellman, *Annu. Rev. Cell Biol.*, 1989, **5**, 483–525.
10 E. J. Blott and G. M. Griffiths, Secretory lysosomes, *Nat. Rev. Mol. Cell Biol.*, 2002, **3**, 122–131.
11 J. Stinchcombe, G. Bossi and G. M. Griffiths, *Science*, 2004, **305**, 55–59.
12 M. Schindler, S. Grabski, E. Hoff and S. M. Simon, *Biochemistry*, 1996, **35**, 2811–2817.
13 R. T. Kennedy, L. Huang and C. A. Aspinwall, *J. Am. Chem. Soc.*, 1996, **118**, 1795–1796.
14 R. Martínez-Zaguilán, B. F. Chinnock, S. Wald-Hopkins, M. Bernas, D. Way, M. Weinand, M. H. Witte and R. J. Gillies, *Cell. Physiol. Biochem.*, 1996, **6**, 169–184.
15 H. Galster, *pH Measurement: Fundamentals, Methods, Applications, and Instrumentation*. VCH, New York. 1991.
16 F. B. M. Suah, M. Ahmad and M. N. Taib, *Sens. Actuators, B*, 2003, **90**, 182–188.
17 J. Qi, D. Liu, X. Liu, S. Guan, F. Shi, H. Chang, H. He and G. Yang, *Anal. Chem.*, 2015, **87**, 5897–5904.
18 J. Han and K. Burgess, *Chem. Rev.*, 2010, **110**, 2709–2728.
19 S. Charier, O. Ruel, J. B. Baudin, D. Alcor, J. F. Allemand, A. Meglio and L. Jullien, *Angew. Chem., Int. Ed.*, 2004, **43**, 4785–4788.
20 M. Su, Y. Liu, H. Ma, Q. Ma, Z. Wang, J. Yang and M. Wang, *Chem. Commun.*, 2001, 960–961.
21 A. Lobnik, I. Oehme, I. Murkovic and O. S. Wolfbeis, *Anal. Chim. Acta*, 1998, **367**, 159–165.
22 D. A. Nivens, M. V. Schiza and S. M. Angel, *Talanta*, 2002, **58**, 543–550.
23 J. Ji and Z. Rosenzweig, *Anal. Chim. Acta*, 1999, **397**, 93–102.
24 O. S. Wolfbeis, *Anal. Chem.*, 2000, **72**, 81–89.
25 D. Aigner, B. Ungerböck, T. Mayr, R. Saf, I. Klimant and S. M. Borisov, *J. Mater. Chem. C*, 2013, **1**, 5685–5693.
26 K. H. Knauer and R. Gleiter, *Angew. Chem., Int. Ed. Engl.*, 1977, **16**, 113.
27 X. He, F. Ding, W. Xua, C. Xua, Y. Lia, Y. Qian, S. Zhao, H. Chen and J. Shen, *Anal. Chim. Acta*, 2020, **1127**, 29–38.
28 Z. Ding, G. Liu and J. Hu, *Biomacromolecules*, 2020, **21**, 3436–3446.
29 J. Wang, X. Wang, X. Pan, W. Pan, Y. Li, X. Liang and X. Sun, *Microchim. Acta*, 2020, **187**, 330.
30 J. Wang, S. Xia, J. Bi, Y. Zhang, M. Fang, R. L. Luck, Y. Zeng, T.-H. Chen, H. M. Lee and H. Liu, *J. Mater. Chem. B*, 2019, **7**, 198–209.
31 Y. Yang, Q. Zhao, W. Feng and F. Li, *Chem. Rev.*, 2013, **113**, 192–270.
32 Y. E. Koo Lee, R. Kopelman and R. Smith, *Annu. Rev. Anal. Chem.*, 2009, **2**, 57–76.
33 J. Chao, Y. Liu, J. Sun, L. Fan, Y. Zhang, H. Tong and Z. Li, *Sens. Actuators, B*, 2015, **221**, 427–433.
34 A. Arroyo-Pieck, D. Araiza-Olivera and J. Peon, *Chem. Plus. Chem.*, 2018, **83**, 1097–1108.
35 D. Wencel, T. Abel and C. McDonagh, *Anal. Chem.*, 2014, **86**, 15–29.
36 M. S. Briggs, D. D. Burns, M. E. Cooper and S. J. Gregory, *Chem. Commun.*, 2000, 2323–2324.
37 J. E. Mathejczyk, J. Pauli, C. Dullin, U. Resch-Genger, F. Alves and J. Napp, *J. Biomed. Opt.*, 2012, **17**, 076028.
38 C. Wang, S. Otto, M. Dorn, K. Heinze and U. Resch-Genger, *Anal. Chem.*, 2019, **91**, 2337–2344.
39 M. Meldal and C. Wenzel Tornøe, Cu-Catalyzed Azide–Alkyne Cycloaddition, *Chem. Rev.*, 2008, **108**, 2952–3015.
40 X. Chen, T. Pradhan, F. Wang, J. S. Kim and J. Yoon, *Chem. Rev.*, 2012, **112**, 1910–1956.
41 Z. Li, Y. Song, Y. Yang, L. Yang, X. Huang, J. Han and S. Han, *Chem. Sci.*, 2012, **3**, 2941–2948.
42 H. Montenegro, M. Di Paolo, D. Capdevila, P. F. Aramendía and M. L. Bossi, *Photochem. Photobiol. Sci.*, 2012, **11**, 1081–1086.
43 M. Tian, X. Peng, J. Fan, J. Wang and S. Sun, *Dyes Pigm.*, 2012, **95**, 112–115.
44 Z. Hu, M. Li, M. Liu, W. Zhuang and G. Li, *Dyes Pigm.*, 2013, **96**, 71–75.
45 H. S. Lv, J. Liu, B. X. Zhao and J. Y. Miao, *Sens. Actuators, B*, 2013, **177**, 956–963.
46 H. Beens, H. Knibbe and A. Weller, *J. Chem. Phys.*, 1967, **47**, 1183–1184.
47 E. M. S. Castanheira and J. M. G. Martinho, *J. Photochem. Photobiol., A*, 1994, **80**, 151–156.
48 F. D. Lewis and E. L. Burch, *J. Photochem. Photobiol., A*, 1996, **96**, 19–23.
49 I. B. Berlman, *Handbook of Fluorescence Spectra of Aromatic Molecules*, Academic Press Inc., New York. NY, 1965.
50 W. R. Dawson and M. W. Windsor, *J. Phys. Chem.*, 1968, **72**, 3251–3260.
51 H. T. S. Britton and R. A. Robinson, *Chem. Soc.*, 1931, 1456.
52 S. Radunz, E. Andresen, C. Würth, A. Koerdt, H. R. Tschiche and U. Resch-Genger, *Anal. Chem.*, 2019, **91**, 7756–7764.
53 M. Taniguchi and J. S. Lindsey, *Photochem. Photobiol.*, 2018, **94**, 290–327.
54 PBEh-3c, DOI: 10.1063/1.4927476.
55 TM, DOI: 10.1016/0009-2614(89)85118-8.
56 COSMO, DOI: 10.1039/P29930000799.
57 ORBKIT, DOI: 10.1002/jcc.24358.
58 L. Exbrayat, S. Salaluk, M. Uebel, R. Jenjob, B. Rameau, K. Koynov, K. Landfester, M. Rohwerder and D. Crespy, *ACS Appl. Nano Mater.*, 2019, **2**, 812–818.
59 D. Si, T. Epstein, Y.-E. Koo Lee and R. Kopelman, *Anal. Chem.*, 2012, **84**, 978–986.
60 T. Behnke, J. E. Mathejczyk, R. Brehm, C. Würth, F. R. Gomes, C. Dullin, J. Napp, F. Alves and U. Resch-Genger, *Biomaterials*, 2013, **34**, 160–170.

